J Nanopart Res (2015) 17:400
DOI 10.1007/s11051-015-3204-1

RESEARCH PAPER

# The interactions between humic acids and Pluronic F127 produce nanoparticles useful for pharmaceutical applications

**Bruna Alice Gomes de Melo · Fernanda Lopes Motta · Maria Helena Andrade Santana**

Received: 21 July 2015 / Accepted: 28 September 2015 / Published online: 8 October 2015


**Abstract** Humic acids (HAs) are macromolecules composed of a large variety of functional groups including phenols and carboxylic acids, which have anti-inflammatory and antioxidant properties. HAs are completely soluble in aqueous medium in alkaline conditions only. At neutral pH, the protonation of the OH/OOH groups causes the formation of micelle-like structures containing a hydrophobic core. Pluronic F127 (PF127) is a nonionic and non-toxic block copolymer with surfactant properties, which are able to interact with HAs through hydrophobic interactions. In this work, these interactions were studied to determine the potential of HA–PF127 structures for pharmaceutical applications. The HAs used was composed of phenol (15.92 %), carboxylic (13.70 %), and other aromatic groups as characterized by $^{13}C$ NMR, GC–MS, and FTIR. Initially, the HA–PF127 interactions were identified by a fivefold decrease in the CMC of PF127. The effects of the HA:PF127 molar ratio were studied by adding naturally occurring HAs to PF127 dispersions under mechanical stirring. The highest ratios, 1:8 and 1:80, favored the formation of submicellar aggregates of approximately 100 nm and zeta potentials of −28.37 and −30.23 mV, respectively. HA–PF127 structures were spherical, with a polydispersity of approximately 0.43. These results show that the interactions between HAs and PF127 produce stable nanoparticles. These nanoparticles may be used as a carrier for hydrophobic bioactives and as an antioxidant or anti-inflammatory agent. To the best of our knowledge, this work is the first attempt to develop HA–PF127 nanoparticles.

**Keywords** Humic acids · Pluronic F127 · Nanoparticles · Pharmaceutical application · Anti-inflammatory agent · Drug carrier

B. A. G. de Melo · F. L. Motta · M. H. A. Santana (✉)
Development of Biotechnological Processes Laboratory, School of Chemical Engineering, University of Campinas, Campinas, São Paulo 13083-852, Brazil
e-mail: mariahelena.santana@gmail.com

## Introduction

Humic substances (HS) are organic matter originated from the decay of vegetable and natural residues in terrestrial soil, natural water, and sediment (Maccarthy 2001). HS are comprised by three different fractions: humines, fulvic acids, and humic acids (HAs).

HAs are macromolecules with undefined chemical compositions that vary with the origin and conditions of their extraction/production. HAs contain numerous functional groups including carboxylic acid, phenol, enol, alcohol, quinone, ether, and others (Sposito 1986; Stevenson 1982). The OH groups correspond to the hydrophilic portions of HAs, while the aromatic rings and aliphatic chains contribute to their hydrophobic character and give rise to surfactant properties.

The OH/OOH groups in HAs structure are responsible for various properties of these organic acids that are beneficial to human health. When deprotonated, HAs are able to bind cationic sites of a virus, thus inhibiting the virus' attachment to the cell surface and preventing its replication (Neyts et al. 1992). This characteristic is also related to their anti-inflammatory (Junek et al. 2009) and antimutagenic/desmutagenic effects (Ferrara et al. 2006). HAs have many phenolic groups in their structure, which provide antioxidant characteristics. Phenols act as electron donators, scavenging free radicals, preventing chain reactions and binding metals such as iron and copper, therefore inhibiting free radical formation by metal catalysis (Rice-Evans et al. 1997). HAs can also absorb in the UV–visible range and, thus, have potential for use in sunscreens, anti-aging creams, and skin care products in general (Klöcking et al. 2013). In addition to these inherent properties, HAs can complex with hydrophobic compounds, making them soluble in water (Martini et al. 2010).

HAs do not have a defined composition. They are distinguished from the other HS fractions based on water solubility, defined as being in neutral-to-alkaline conditions (Stevenson 1982). In addition to pH, the presence of cations in the medium can affect HAs solubility (Von Wandruszka et al. 1997). In alkaline mediums, HAs are completely soluble because the OH groups are deprotonated, and the repulsion of these negatively charged groups causes the molecules to assume a stretched configuration. With a decrease in pH or the addition of cations to a solution, these negatively charged groups are re-protonated, and the charge repulsion is minimized. This change causes the molecules to coil up and aggregate to form compact structures called pseudomicelles with hydrophobic cores and hydrophilic surfaces (Von Wandruszka et al. 1997; Von Wandruszka 2000). In water, HAs have both soluble and insoluble fractions. According to the mechanisms proposed by Klučáková and Pekař (2005), the soluble fractions of HAs can exist as dissolved molecules and in a dissociated form, while the insoluble fractions can interact with the environment by acting like an ion-exchanger and releasing $H^+$ ions into solution, while the anions remain insoluble.

As amphiphilic molecules, HAs interact with surfactants through hydrophobic and electrostatic interactions (Ishiguro and Koopal 2011; Matsuda et al. 2009; Otto et al. 2003). Otto et al. (2003) demonstrated that HAs decreased twofold the CMC of sodium dodecyl sulfate (SDS), an anionic surfactant, suggesting the formation of submicellar HA–SDS aggregates. Even with the electrostatic repulsion between the two compounds, the hydrophobic interaction was more significant. To our knowledge, no report exists describing interactions between HAs and surfactants for use in pharmaceutical applications.

Pluronic F127 (PF127) is a nonionic surfactant that belongs to the block copolymers group, formed by the triblock structure PEO–PPO–PEO. In this triblock, PEO is poly(ethylene oxide) (the hydrophilic portion), and PPO is poly(propylene oxide) (the hydrophobic portion). Among all the block copolymers, PF127 is one of the least toxic, and has therefore been used for wound and burn healing/treatment for many years (Schmolka 1972). PF127′s low toxicity and high biocompatibility make this surfactant appealing for use as a drug carrier (Foster et al. 2009; Taha et al. 2014). Several previous studies demonstrated that the interaction of PF127 with other surfactants enhances its stability and the permeation and diffusion properties of the active compounds (Antunes et al. 2011; Zhang et al. 2011).

In this work, we studied HA–PF127 interactions with the potential for the technological production of nanoparticles, which are useful alone or as a drug delivery system, for pharmaceutical.

## Materials and methods

### Materials

Both commercial HAs and PF127 were purchased from Sigma-Aldrich (Switzerland). Ultrapure water was used throughout all experimental studies.

### Characterization of solid HAs

#### *Elemental analysis*

Carbon, nitrogen, hydrogen, and sulfur contents were determined quantitatively by combustion bulk elemental analysis using a Fisons-EA-1108 (Thermo Scientific, MA, USA).

*Solid-state $^{13}C$ NMR spectroscopy*

Solid-state $^{13}C$ NMR spectra of HAs were obtained using the high-powered decoupling program (HPDEC) on a Bruker 400 resonating at 100 MHz. The spinning rate was maintained at 10 kHz using a 4 mm Zr rotor.

*Pyrolysis–gas chromatography–mass spectroscopy*

The pyrolysis of HAs was performed in a muffle furnace at 650 °C for 10 min. Vapors generated during the heating were collected with dichloromethane, and the extracted vapors were analyzed using an Agilent 5975C single quadrupole GC–MS with a He flow gas and a HP-5 MS 5 % diphenyl and 95 % dimethylpolysiloxane column (30 m × 0.25 mm × 0.25 μm) was employed in the separation. NIST11 Standard Reference Database was used to identify the compounds detected.

*Fourier transform infrared (FTIR) analysis*

FTIR analysis of solid HAs was performed on a Thermo Scientific Nicolet 6700 spectrophotometer. Pellets were prepared by mixing 2 mg of solid HAs with 200 mg of KBr and pressing the mixture under vacuum at 7 t for 10 min. The wavelength range of the performance was 4000–400 $cm^{-1}$ with a resolution of 4 $cm^{-1}$.

Interactions between PF127 and HAs

*Critical micelle concentration (CMC)*

CMC values of PF127 and HA–PF127 were determined using conductivity measurements in a conductivimeter Digimed DM-32 at room temperature. The PF127 dispersions were prepared at a concentration between 50 and 3000 mg $L^{-1}$ (0.005 and 0.30 %) under magnetic stirring. For HA–PF127 assays, 10 mg $L^{-1}$ of solid HAs were added to the PF127 dispersions under mechanical stirring at 700 rpm and 25 °C for 1 h. Next, the solutions were filtered with 80 g qualitative filter paper to remove the precipitated HAs. The final concentration of the dispersed HAs was 6 mg $L^{-1}$. The assays were performed in triplicate.

*Preparation of HA–PF127 nanoparticles*

Dispersions of PF127 were prepared at the following concentrations: 0.1, 1.0, and 5.0 % w/v. Solid HAs were added to the PF127 dispersions under mechanical stirring at 700 rpm and 25 °C for 1 h. Then, the formed dispersions were filtered with 80 g qualitative filter paper to remove the precipitated HAs. The precipitated fraction contained approximately 40 % of the HA initial mass. Thus, solutions with molar ratios of 1:80, 1:800, and 1:4000 HAs:PF127 were made from 6 mg $L^{-1}$ HAs (10 mg $L^{-1}$ initial HAs). The highest molar ratio (1:8) was made from adding 55 mg $L^{-1}$ HAs (100 mg $L^{-1}$ initial HAs) to a 0.1 % PF127 dispersion. A solution of 10 mg $L^{-1}$ HAs in water and solutions of 0.1, 1.0, and 5.0 % w/v PF127 without HAs were used as controls. The assays were performed in triplicate.

Characterization of the HA–PF127 nanoparticles

*Size, polydispersity index (PDI), and zeta potential*

The size, polydispersity index, and zeta potential of HA–PF127, PF127, and HAs structures were measured using dynamic light scattering (DLS) in an Autosizer 4700, Zetasizer Nano (Malvern). The equipment measured each sample ten times.

*Scanning electron microscopy*

The morphology of the HA–PF nanoparticles (1:80 molar ratio) was verified by scanning electron microscopy (SEM) after drying the sample and coating it with 1.5 nm of iridium. The analysis was carried out using a Quanta FEG 250 microscope operating at an accelerating voltage of 20 kV.

## Results and discussion

Characterization of solid HAs

Due to the variability in HAs composition based on its origin/extraction process, it was necessary to characterize the compound being used in this work. The CNHS elemental analysis of the HAs used in this work provided the following results: 38.13 % of C, 3.21 % of H, 0.66 % of N, and 0.36 % of S. Oxygen and

inorganic constituents composed the remainder of the compound. The results differed from previous studies on HAs from Sigma-Aldrich (Sidiqui et al. 2009), especially in carbon concentration, which the authors characterized as being 55.60 % of the total HA composition. This difference could be due to different sources of extraction or different purity levels of the compound, which were not specified by the supplier.

The functional groups were characterized by solid-state $^{13}C$ NMR spectroscopy and pyrolysis–GC/MS to identify the presence of OH and COOH, which gives HAs its pharmaceutical properties. The $^{13}C$ NMR spectra of the HAs presented in Fig. 1a exhibit peaks corresponding to the chemical shifts of $^{13}C$ from the aliphatic, aromatic, carboxylic, and thiocarbonyl groups in accordance with reports by Pretsch et al. (2000). The presence of aliphatic groups was confirmed by the signal between $\delta$ 50 and 0 ppm, while the presence of aromatic groups was indicated by an intense signal between $\delta$ 160 and 100 ppm. The shoulder in $\delta$ 150 ppm indicates the presence of a phenolic group. The signal between $\delta$ 190 and 160 ppm corresponds to the presence of carboxylic groups in the HAs. There exists a less intense signal in the range of $\delta$ 240–220 ppm that likely corresponds to the thiocarbonyl groups. The resonance integrals of the four peaks are shown in Table 1. Their content was calculated as the sum of the percentages of the peak area for each compound. Aromatic groups corresponded to 56.18 % of the total composition, including phenolic groups, because it was not possible to integrate these groups separately. The aliphatic and carboxylic acids corresponded to 24.77 and 13.70 % of the total composition, respectively, and the thiocarbonyls corresponded to 5.35 % of total peak area.

The GC–MS chromatogram of the pyrolyzed extract of HAs is shown in Fig. 1b. Fifteen peaks were identified, and all of the compounds are listed in Table 2. Their contents were calculated as the sum of the percentages of the peak area for each compound. The carboxylic acids have not been identified because of their thermal degradation in $CO_2$ during the pyrolysis process. The phenolic groups corresponded to 15.92 % of the total composition, while all other aromatics corresponded to 82.05 % of the total composition. The analysis showed that the aliphatic groups correspond to 2.03 % of the total composition. The high content of alkylbenzenes and the low content of aliphatic groups characterized by GC–MS could be explained by thermal degradation of aromatic rings linked to aliphatic chains, which forms aromatic hydrocarbons (Abbt-Braum et al. 1989; Schulten 1987).

Figure 1c shows the FTIR spectrum of solid HAs and was interpreted based on Günzler and Gremlich (2002). The presence of aliphatics was evidenced by two stretching bands of C–H at 2917 and 2848 $cm^{-1}$ and two bending bands at 1380 (in plane) and 1030 $cm^{-1}$ (out of plane). The band at 1030 $cm^{-1}$ could also be attributed to C=S stretching of the thiocarbonyls. At 1615 $cm^{-1}$, we observed a pronounced peak from 1500 to 1800 $cm^{-1}$. Aromatic C=C and C=O stretching bands appear at 1615 $cm^{-1}$; the shoulder at 1700 $cm^{-1}$ may be a result of C=O stretching of carboxylic acids or ketones. As ketones were not identified by the other two methods of characterization, we attributed this shoulder to the presence of carboxylic acids. Carboxylic acids may also account for the stretching vibration bands of C–O in 1093–1030 $cm^{-1}$ region and the bending of C–O–H in plane at 1380 $cm^{-1}$. The C–C vibration in aromatics appears from 1600 to 1585 $cm^{-1}$ and at 690 $cm^{-1}$, and the peak at 912 $cm^{-1}$ corresponds to the C–H deformation in these groups. The hydroxyl stretching bands (3691–3436 $cm^{-1}$) could be a result of phenolic and carboxylic acids present in the compound.

The three methods of characterization were complementary to each other. The FTIR spectrum contained a large peak corresponding to C=C and C=O stretching bands of aromatic and phenolic/carboxylic groups, because neither $^{13}C$ NMR nor GC–MS indicated the presence of ketones in HAs. The low-intensity peaks of aliphatics compared to aromatics in FTIR were in agreement with the other methods of characterization. Using $^{13}C$ NMR and GC–MS, we determined that carboxylic acids and phenols account for 13.70 and 15.92 %, respectively, of the total HAs. These results are in agreement with the values found in the literature for HAs from Sigma-Aldrich (Baigorri et al. 2009; Shin et al. 1999). Thus, approximately 70.00 % of the HAs are composed by hydrophobic components, which contribute to the nonpolar core of the HAs structures in water.

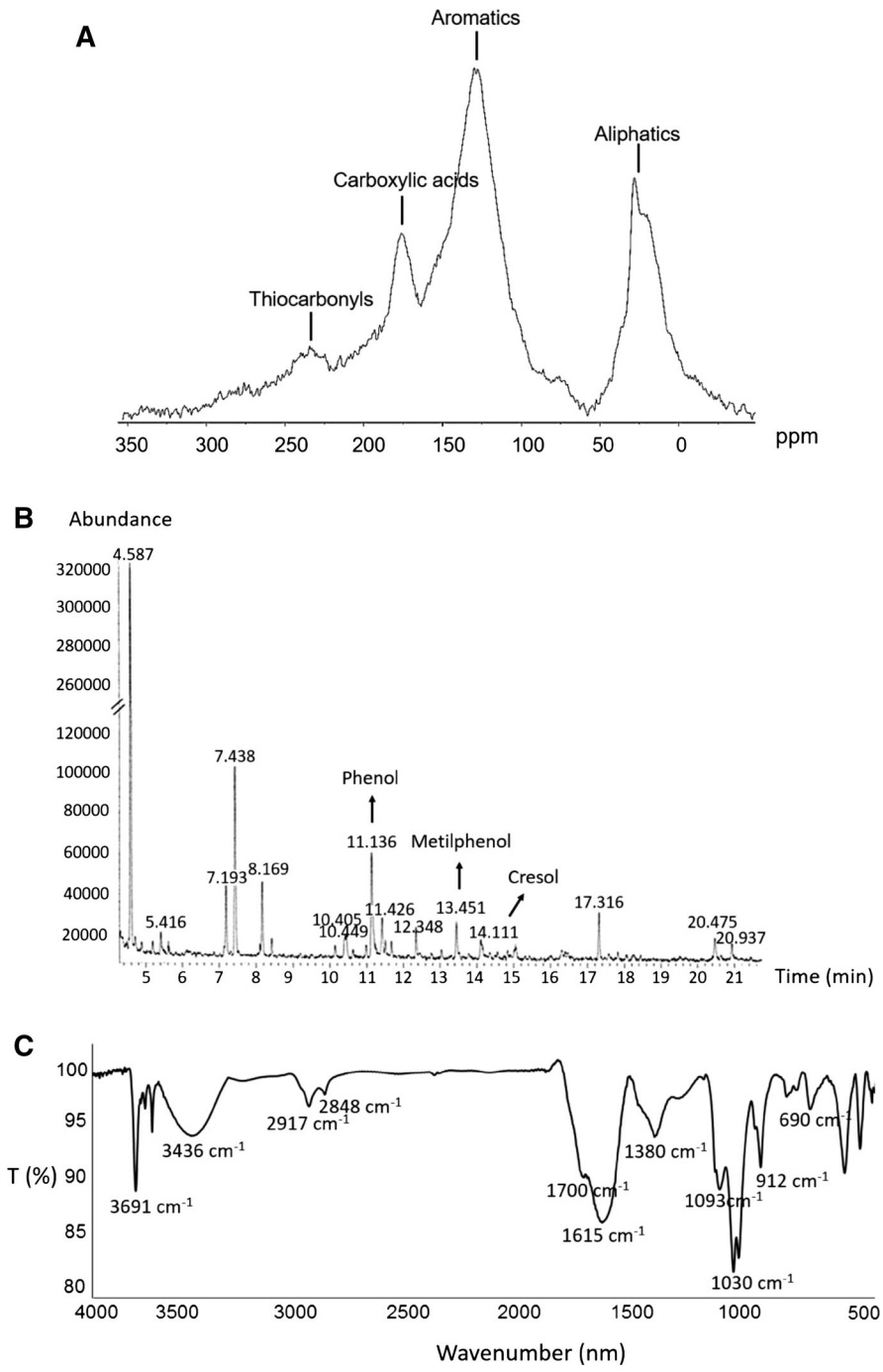


**Fig. 1** Characterization of HAs used in this study. $^{13}C$ NMR spectrum (**a**). The chromatogram of GC–MS of the pyrolyzed extract of the HAs (**b**). FTIR spectrum (**c**)

**Table 1** Relative intensity distribution and chemical shift of the functional groups in the $^{13}C$ NMR spectra of the HA used in this study

| Functional group | Chemical shift (ppm) | Relative intensity (%) |
|---|---|---|
| Thiocarbonyl | 240–220 | 5.35 |
| Carboxylic acid | 190–160 | 13.70 |
| Aromatic | 160–100 | 56.18 |
| Aliphatic | 50–0 | 24.77 |

**Table 2** Time retention, abundance, and the base m/z of the compounds obtained by pyrolysis–GC/MS of the HAs used in this study

| Compound | $R_t$ (min) | Abundance (%) | Base (m/z) |
|---|---|---|---|
| Toluene | 4.58 | 38.42 | 91 |
| Dimethylhexane | 5.41 | 2.03 | 57, 114 |
| Ethylbenzene | 7.19 | 5.92 | 91, 106 |
| Xylene (isomer) | 7.43 | 14.27 | 91, 106 |
| Xylene (isomer) | 8.16 | 5.66 | 91, 106 |
| Methyl-ethylbenzene (isomer) | 10.40 | 2.13 | 105, 120 |
| Methyl-ethylbenzene (isomer) | 10.44 | 1.88 | 105, 120 |
| Phenol | 11.13 | 11.05 | 66, 94 |
| Trimethylbenzene (isomer) | 11.42 | 2.90 | 105, 120 |
| Trimethylbenzene (isomer) | 12.34 | 2.46 | 105, 120 |
| Methylphenol | 13.45 | 2.76 | 79, 90, 108 |
| Cresol | 14.11 | 2.11 | 77, 91, 108 |
| Naphthalene | 17.31 | 4.04 | 102, 128 |
| Methylnaphthalene (isomer) | 20.47 | 2.85 | 115, 141 |
| Methylnaphthalene (isomer) | 10.93 | 1.45 | 115, 141 |

## Interactions between PF127 and HAs

### *Critical micelle concentration (CMC)*

The interactions between PF127 and HAs were initially studied using CMC determinations of PF127 and HA–PF127 using electrical conductivity measurements. The abrupt change in the slope marked 'CMC' is shown in Fig. 2. The CMC value for PF127 was 822 mg $L^{-1}$ (0.082 %), which was comparable with previously reported values (Sezgin et al. 2006; Vasilescu and Bandula 2011). The CMC for HA–PF127 was 160 mg $L^{-1}$ (0.016 %). In other words, there was a fivefold decrease in the CMC value compared with PF127 without HAs. After the addition of 10 mg $L^{-1}$ HAs, approximately 4 mg $L^{-1}$ precipitated in all assays (40 %). Therefore, PF127 only interacted with HAs in micelle-like structures.

The interactions between humic materials and surfactants were previously studied by Otto et al. (2003). The authors showed that the HS enhanced the aggregation of SDS prior to micellization, causing more significant hydrophobic effects. Furthermore, stable ion pairs were formed between the positively charged cetyltrimethylammonium bromide (CTAB) and the humic substances.

### *The effects of various AH/PF127 ratio*

Figures 3 shows the Intensity ($I\alpha d^6$) and Number ($N\alpha d$) distributions of hydrodynamic diameters obtained using light scattering for HAs, PF127 dispersions and HA–PF127 structures as function of the initial PF127 concentration. Table 3 presents the zeta potential for the same samples.

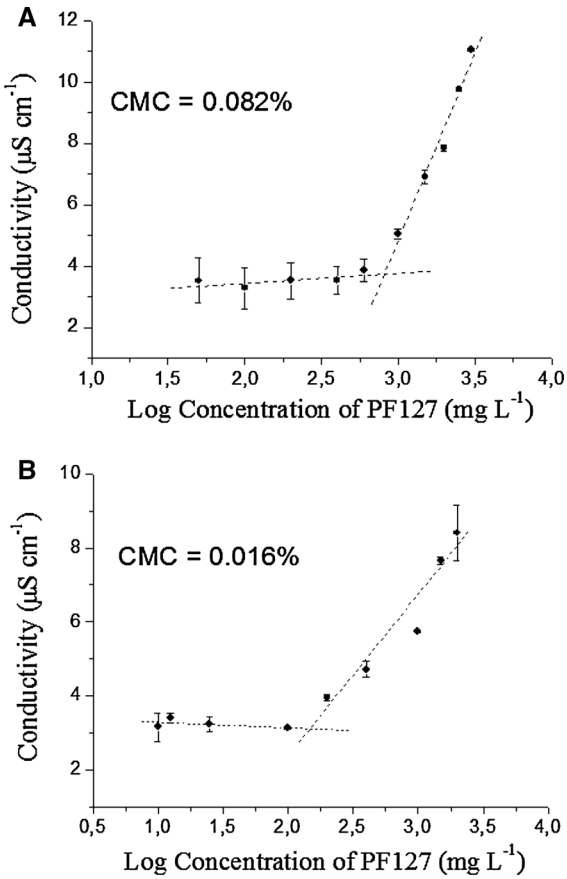


**Fig. 2** CMC determinations of PF127 and HA–PF127. PF127 (**a**). HA–PF127 (**b**)

Figure 3a, b correspond to the HAs micelle-like structures formed in water. The distribution of the diameter ranged from approximately 100–1000 nm, with a maximum at approximately 300 nm. In addition, a small population of micelle-like structures with a diameter of approximately 10,000 nm was also detected. From the I$\alpha d^6$, the calculated predominant mean diameter was 342 nm, according to the N$\alpha$d.

Figure 3c shows the diameters of PF127 0.1 % micelles ranged from 10 to 100 nm. The presence of HAs in the 1:80 ratio of HA:PF127 greatly reduced the peak at approximately 10 nm and slightly shifted the peak of HA pseudomicelles from 100–1000 to 100–500 nm, suggesting the formation of mixed micelles with PF127. However, the N$\alpha$d (Fig. 3d) shows that 5 nm PF127 micelles predominate in the dispersion. Figure 3e, f suggest a slight incorporation of PF127 in HA micelle-like structures in the 1:800 ratio, forming HA–PF127 structures with sizes ranging from 100 to 600 nm and the predominance of 5 nm PF127 micelles in the dispersion. At the ratio 1:4000 (Fig. 3g, h), the I$\alpha d^6$ peaks corresponding to surfactant micelles were maintained or suffered only minor changes, while populations with large diameters appeared throughout the range of 100–10,000 nm. In this experiment, higher surfactant concentrations may have induced the formation of intermolecular bonds without interacting with the HA micelle-like structures. Similar to experiments with ratios of 1:80 and 1:800, the N$\alpha$d suggests that the main population in the dispersion consists of PF127 micelles.

Finally, Fig. 3i, j represent the highest HA–PF127 ratio (1:8). The I$\alpha d^6$ suggests a decrease in the number of PF127 micelles and the incorporation of the surfactant in HA pseudomicelles. This may be due to hydrophobic interactions between the aromatic groups in HAs and the PPO from the surfactant. The N$\alpha$d shows that for this ratio, the predominant population in the dispersion consists of HA–PF127 structures with a diameter of approximately 100 nm. These results suggest that interactions between HAs and PF127 may reinforce tight packing and form a cohesive core in HA–PF127 structures (Lee et al. 2011; Manaspon et al. 2012). With a more hydrophobic core, these nanoparticles will be more likely to entrap nonpolar bioactive compounds (Owen et al. 2012; Wei et al. 2009).

In addition to the diameter distributions, the presence of HAs increased the polydispersity of the PF127 micelles from values of approximately 0.27–0.43 at 0.1 and 1.0 %, confirming the described interactions.

Table 3 shows the results from zeta potential analysis. Slightly negatives values (−3.25 mV) were measured for HAs at 6 mg $L^{-1}$ and higher values (−32.03 mV) for HAs at 55 mg $L^{-1}$, indicating a direct effect on zeta potential that is likely due to the presence of $OH^-/OOH^-$ groups. Slightly negative values were measured for PF127 micelles that indicated low stability of the dispersions, which are prone to aggregation. The addition of HAs in the PF127 dispersions in ratios of 1:8, 1:80, and 1:800 results in high negative values of zeta potential of −28.37, −30.23, and −15.52 mV, respectively. This indicates that the surfactant interacts with HAs pseudomicelles as shown in Fig. 4 and that the zeta potential value may be exclusively affected by HAs. At the lowest

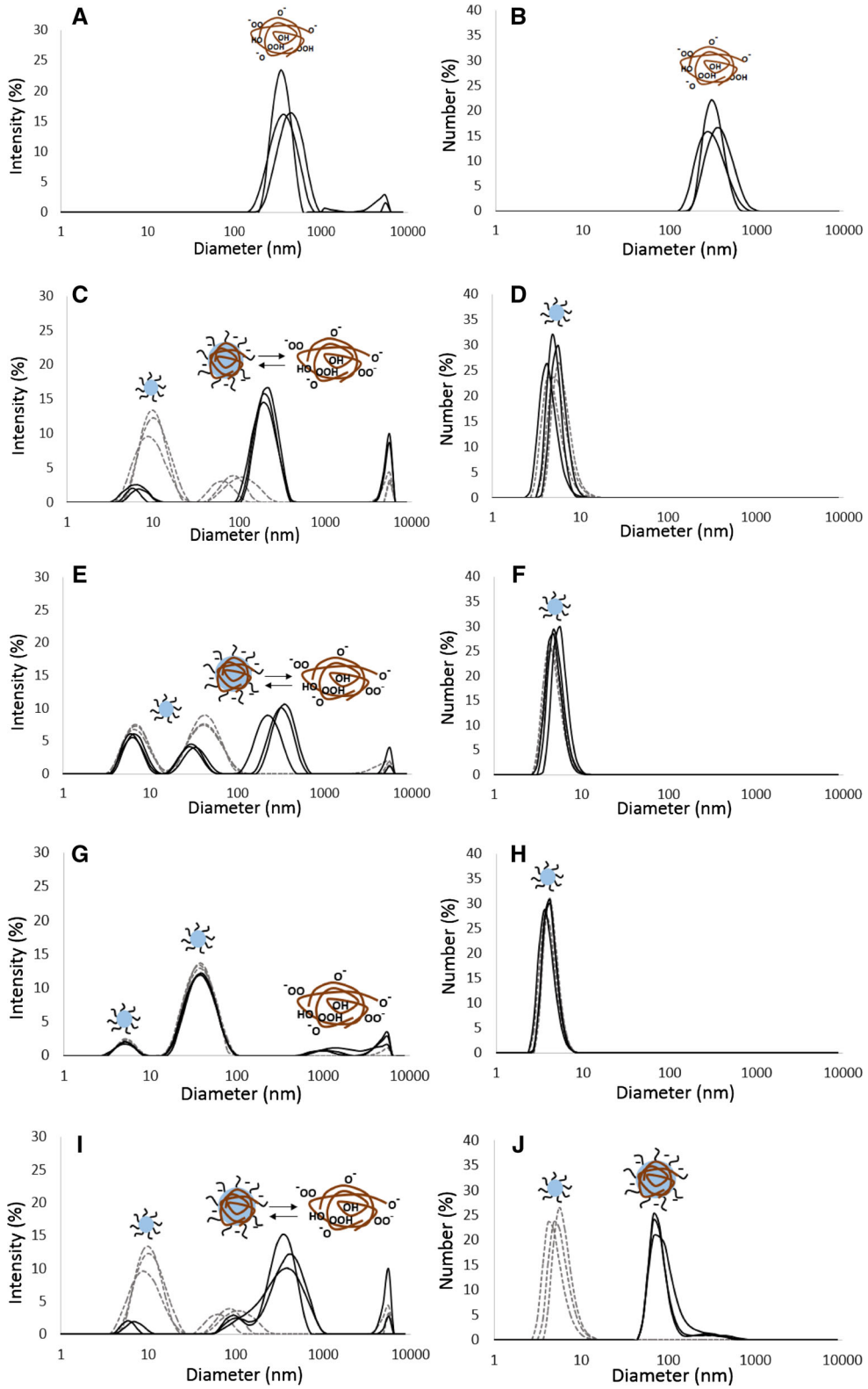
A
B
C
D
E
F
G
H
I
J
Intensity (%)
Number (%)
Diameter (nm)
1
10
100
1000
10000

◀**Fig. 3** Intensity and number distributions for hydrodynamic diameter obtained from light scattering. HAs 6 mg $L^{-1}$ (**a**). For **c– j**: PF127 0.1, 1.0, and 5.0 % (*dashed line*) and HA–PF127 (*thick line*). Ratio HA:PF (mol/mol) 1:80 (**a** and **b**). 1:800 (**c** and **d**). 1:4000 (**e** and **f**). 1:8 (**g** and **h**). The data represent the average measurements of each triplicate assay

ratio (1:4000), the zeta potential value corresponds to the micelle structures of PF127 due to their excess in the dispersion.

**Table 3** Zeta potential of HAs, PF127 dispersions at concentrations 0.1, 1.0, and 5.0 % w/v, and HA–PF127 for the different ratios HA:PF127

| Structure | Zeta potential (mV) |
|---|---|
| HAs | |
| 6 mg $L^{-1}$ | −3.25 ± 0.71 |
| 55 mg $L^{-1}$ | −32.03 ± 5.29 |
| PF127 in water | |
| 0.1 % | −3.71 ± 1.00 |
| 1.0 % | −6.02 ± 0.64 |
| 5.0 % | −3.96 ± 1.61 |
| HA:PF127 ratio (mol:mol) | |
| 1:8 | −28.37 ± 6.17 |
| 1:80 | −30.23 ± 3.88 |
| 1:800 | −15.52 ± 3.69 |
| 1:4000 | −4.68 ± 1.97 |

Figure 4 illustrates the probable interaction between HAs and PF127 in HA–PF127 structures. Initially, PF127 self-assembles into micelles because it is above its CMC. The soluble fraction of HAs in aqueous solution undergoes intermolecular disaggregation due to the charge repulsion caused by the deprotonation of some of the OH/OOH groups at neutral pH (Klučáková and Pekař 2005; Von Wandruszka et al. 1997; Von Wandruszka 2000). The non-stable micelles of PF127 in water interact with HAs mainly through hydrophobic interactions, as previously reported for hydrophobic drugs (Lee et al. 2011; Zhang et al. 2011). These hydrophobic interactions contributed to the larger and more hydrophobic core of HA–PF127 than HAs alone, which may enhance their ability to entrap nonpolar drugs and to act as a novel alternative to existing nanoparticles for drug delivery.

A synergistic effect could be achieved from the encapsulation of drugs that have effects found in HAs, such as antioxidant and anti-inflammatory activity. It is expected that HAs could enhance these activities and result in lowering the required concentration of administered drugs.

Figure 5 shows the morphology of the HA–PF127 structures for the molar ratio of 1:80 obtained via SEM. The images show non-aggregated spherical structures, with diameters of approximately 70–100 nm, corresponding to the presence of HA–

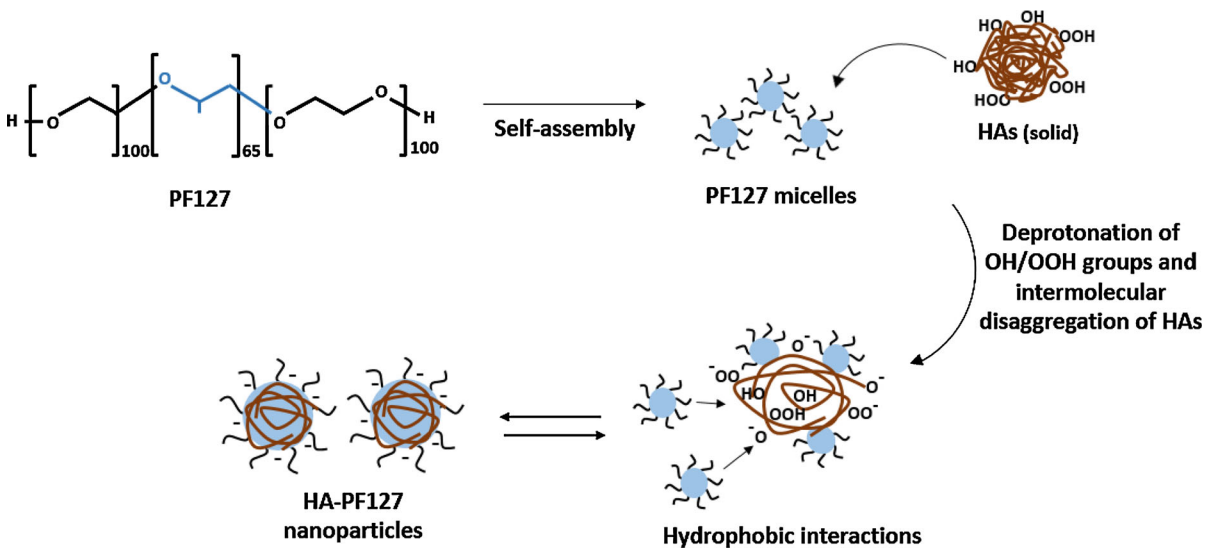


**Fig. 4** Schematic illustration of the interaction between PF127 micelles and HAs micelle-like structures, and the formation of HA–PF127 nanoparticles

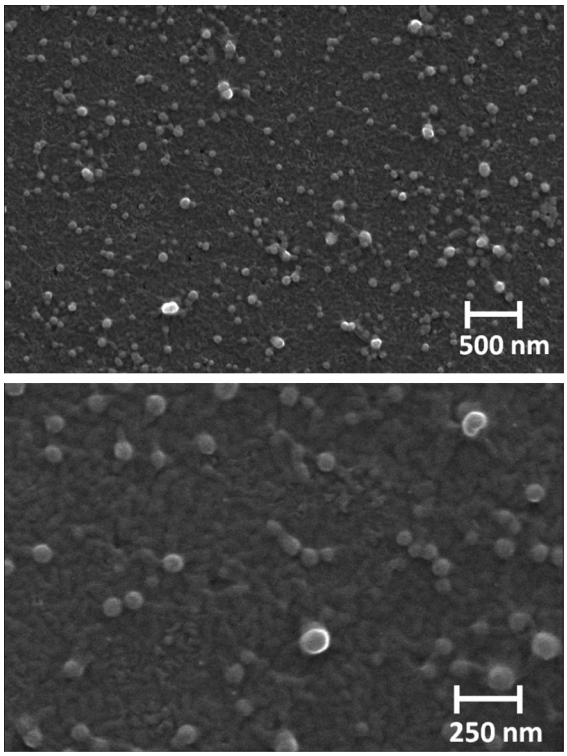


**Fig. 5** Scanning electron microscopy of HA–PF127 structures formed in water for the molar ratio HA:PF127 of 1:80

PF127 structures in equilibrium with HAs pseudomicelles and PF127 micelles.

As expected, the sizes of HA–PF127 were higher from DLS compared with SEM images. This is due to the fact that DLS measures hydrodynamic diameters, which are greater than the actual diameters of the particles (Sokolova et al. 2011).

Together, these results show that the HA–PF127 structures are electrostatically stable nanoparticles. They could potentially act as antioxidant or anti-inflammatory agents and entrap hydrophobic bioactive compounds in their cohesive core.

## Conclusions

The $^{13}C$ NMR, GC–MS and FTIR analysis showed that phenols and carboxylic groups were present in the HAs used in this work, indicating their potential to act as antioxidant and anti-inflammatory agents. The interactions between the HAs and PF127 were more favorable when higher HA:PF127 ratios were used and produced spherical and electrostatically stable nanoparticles with a hydrophobic core. The results showed that the HA–PF127 nanoparticles are promising for pharmaceutical applications and for entrapping bioactive compounds.

**Acknowledgments** This work was supported by CNPq (Conselho Nacional de Desenvolvimento Científico e Tecnológico) and Fapesp (Fundação de Amparo à Pesquisa do Estado de São Paulo).

## References

Abbt-Braum G, Frimmel FH, Schulten HR (1989) Structural investigations of aquatic humic substances by pyrolysis field ionization mass spectrometry and pyrolysis gas chromatography/mass spectrometry. Water Res 23(12):1579–1591

Antunes FE, Gentilea L, Rossi CO, Tavanoc L, Ranieri GA (2011) Gels of Pluronic F127 and nonionic surfactants from rheological characterization to controlled drug permeation. Colloid Surf B 87:42–48

Baigorri R, Fuentes M, González-Gaitano G, García-Mina JM, Almendros G, González–Vila FJ (2009) Complementary multianalytical approach to study the distinctive structural features of the main humic fractions in solution: gray humic acid, brown humic acid, and fulvic acid. J Agric Food Chem 57(8):3266–3272

Ferrara G, Loffredo E, Senesi N, Marcos R (2006) Humic acids reduce the genotoxicity of mitomycin C in the human lymphoblastoid cell line TK6. Mutat Res 603:27–32

Foster B, Cosgrove T, Hammouda B (2009) Pluronic triblock copolymer systems and their interactions with ibuprofen. Langmuir 25(12):6760–6766

Günzler H, Gremlich HU (2002) IR spectroscopy. An introduction. Wiley-VCH Verlag GmbH, Weinheim

Ishiguro M, Koopal LK (2011) Predictive model of cationic surfactant binding to humic substances. Colloid Surf A 379:70–78

Junek R, Morrow R, Schoenherr JI, Schubert R, Kallmeyer R, Phull S, Klöcking R (2009) Bimodal effect of humic acids on the LPS-induced TNF-α release from differentiated U937 cells. Phytomedicine 16:470–476

Klöcking R, Felber Y, Guhr M, Meyer G, Schubert R, Schoenherr JI (2013) Development of an innovative peat lipstick based on the UV-B protective effect of humic substances. Mires Peat 11(3):1–9

Klučáková M, Pekař M (2005) Solubility and dissociation of lignitic humic acids in water suspension. Colloid Surf A 252:157–164

Lee ES, Oh YT, Youn YS, Nam M, Park B, Yun J, Kim JH, Song HT, Oh KT (2011) Binary mixing of micelles using Pluronics for a nano-sized drug delivery system. Colloid Surf B 82:190–195

Maccarthy P (2001) The principles of humic substances. Soil Sci 166:738–751

Manaspon C, Viravaidya-Pasuwat K, Pimpha N (2012) Preparation of folate-conjugated Pluronic F127/chitosan core-

shell nanoparticles encapsulating doxorubicin for breast cancer treatment. J Nanomater 100(2):247–256
Martini S, D'addario C, Bonechi C, Leone G, Tognazzi A, Consumi M, Magnani A, Rossi C (2010) Increasing photostability and water solubility of carotenoids: synthesis and characterization β-carotene-humic acids complexes. J Photoch Photobio B 101:355–361
Matsuda M, Kaminaga A, Hayakawa K, Takisawa N, Miyajima T (2009) Surfactant binding by humic acids in the presence of divalent metal salts. Colloid Surf A 347:45–49
Neyts J, Snoeck R, Wutzler P, Cushman M, Klöcking R, Helbig B, Wang P, De Clercq E (1992) Poly(hydroxy)carboxylates as selective inhibitors of cytomegalovirus and herpes simplex virus replication. Antivir Chem Chemoth 3:215–222
Otto WH, Britten DJ, Larive CK (2003) NMR diffusion analysis of surfactant–humic substance interactions. J Colloid Interface Sci 261:508–513
Owen SC, Chan DPY, Shoichet MS (2012) Polymeric micelle stability. Nano Today 7:53–65
Pretsch E, Bühlmann P, Affolter C (2000) Structure determination of organic compounds: tables of spectral data, 3rd edn. Springer, Berlin
Rice-Evans CA, Miller NJ, Paganga G (1997) Antioxidant properties of phenolic compounds. Trends Plant Sci 2(4):152–159
Schmolka IK (1972) Artificial skin I. Preparation and properties of Pluronic F-127 gels for treatment of burns. J Biomed Mater Res 6:571–582
Schulten HR (1987) Time-resolved pyrolysis field ionization mass spectrometry of humic material isolated from freshwater. Environ Sci Technol 21:349–357
Sezgin Z, Yüksel N, Baykara T (2006) Preparation and characterization of polymeric micelles for solubilization of poorly soluble anticancer drugs. Eur J Pharm Biopharm 64:261–268
Shin HS, Monsallier JM, Choppin GR (1999) Spectroscopic and chemical characterizations of molecular size fractionated humic acid. Talanta 50:641–647
Sidiqui Y, Meon S, Ismail R, Rahmani M, Ali A (2009) In vitro fungicidal activity of humic acid fraction from oil palm compost. J Agric Biol 11:448–452
Sokolova V, Ludwig AK, Hornung S, Rotan O, Horn PA, Epple M, Giebel B (2011) Characterisation of exosomes derived from human cells by nanoparticle tracking analysis and scanning electron microscopy. Colloid Surf B 87:146–150
Sposito G (1986) Sorption of trace metals by humic materials in soils and natural waters. Crit Rev Environ Sci Technol 16:193–229
Stevenson FJ (1982) Humus chemistry. John Wiley, New York
Taha EI, Badran MM, El-Anazi MH, Bayomi MA, El-Bagory IM (2014) Role of Pluronic F127 micelles in enhancing ocular delivery of ciprofloxacin. J Mol Liq 199:251–256
Vasilescu M, Bandula R (2011) Aggregation of Pluronic F127 and polydimethylsiloxane-graft-polyether block copolymers in water and microstructure of aggregates as evaluated by molecular probe techniques. Rev Roum Chim 56(1):57–64
Von Wandruszka R (2000) Humic acids: their detergent qualities and potential uses in pollution remediation. Geochem Trans 1:10. doi:10.1186/1467-4866-1-10
Von Wandruszka R, Ragle C, Engebretson R (1997) The role of selected cations in the formation of pseudomicelles in aqueous humic acid. Talanta 44:805–809
Wei Z, Hao J, Yuan S, Li Y, Juan W, Sha X, Fang X (2009) Paclitaxel-loaded Pluronic P123/F127 mixed polymeric micelles: formulation, optimization and in vitro characterization. Int J Pharm 376:176–185
Zhang W, Shi Y, Chen Y, Ye J, Sha X, Fang X (2011) Multifunctional Pluronic P123/F127 mixed polymeric micelles loaded with paclitaxel for the treatment of multidrug resistant tumors. Biomaterials 32:2894–2906